Turkish Journal of Zoology

http://journals.tubitak.gov.tr/zoology/

Research Article

Turk J Zool
(2026) 50: 94-105
doi:10.55730/1300-0179.3254

Chlorella vulgaris measurements using full-spectrum goniometer for optically complex inland water monitoring

Pınar GÜRBÜZER[1,2,*], **Uğur Murat LELOĞLU**[2]

[1]Department of Hydrobiology, Fisheries Faculty, Sinop University, Sinop, Turkiye

[2]Department of Astronautical Engineering, Faculty of Aeronautics and Astronautics, University of Turkish Aeronautical Association, Ankara, Turkiye

Received: 05.11.2025 • **Accepted/Published Online:** 26.01.2026 • **Final Version:** 26.02.2026

Abstract: Rising environmental stressors, including climate change, nutrient loading, pollution, and anthropogenic impacts, have made the continuous monitoring of lake water quality increasingly essential. While in situ methods offer high precision, satellite-based remote sensing is essential for capturing large-scale, long-term changes and accessing remote or extreme environments. To complement these approaches, we developed a cost-effective in situ optical measurement system specifically designed for optically complex inland waters. The instrument enables detailed optical characterization across scattering angles from 0° to 160° and wavelengths between 423 and 728 nm, covering both visible and near-infrared regions. Initial validation was performed using monocultures of *Chlorella vulgaris*, a well-established model organism for chlorophyll-a optical studies. As a result of laboratory measurements of *C. vulgaris* monocultures using a spectral goniometer, forward and backward scattering profiles, polarization characteristics, three-dimensional patterns, volume scattering functions, and radiant intensities at 90° across Sentinel-3 OLCI bands toward density changes were modeled. The results confirmed Mie scattering dominance in line with the theoretical expectations. Overall, the developed full-spectrum goniometer can serve as a reliable and practical tool for in situ optical monitoring.

Key words: Optical properties, light scattering, phytoplankton, phase function, remote sensing

1. Introduction

Increasing environmental pressures such as climate change, nutrient enrichment, various pollutants, and human activities make the monitoring of lake water quality increasingly critical (Dörnhöfer et al., 2016). Ecosystem services are dependent on sustaining healthy lake ecosystems, and as lakes are subjected to more environmental stresses, it is particularly critical to evaluate their ecological conditions (Wei et al., 2025; Woolway et al., 2025). The continuous monitoring of ecological conditions has become essential for effective management strategies. Satellite-based remote sensing offers significant benefits for viewing remote areas and extreme conditions, as well as for carrying out large-scale and long-term environmental assessments, while in situ methods offer high accuracy and detailed data. Inland waters, which are optically more complex than oceans, require solutions that are more elaborate than current methods, and these solutions must integrate empirical, physical, and technological approaches to effectively address the challenges (Schiller and Doerffer, 1999; Werther et al., 2025).

In aquatic environments, the apparent color and the inherent optical properties (IOPs) of the water column are determined by the combined effect of colored dissolved organic matter (CDOM), phytoplankton pigmentation, and suspended sediments (Brezonik et al., 2005; Adjovu et al., 2023). Among these factors, phytoplankton are of particular importance because they constitute the primary food source for many organisms in aquatic ecosystems. They also play a pivotal role in carbon sequestration and exert strong controls on biogeochemical cycles in inland and marine waters (Robinson, 2017). *Chlorella vulgaris* has become a model for microalgae for both fundamental research and industrial uses because of its rapid growth, broad environmental tolerance, and rich biochemical contents, including lipids, proteins, and pigments (Safi et al., 2014). The well-characterized cellular ultrastructure and optical responses of *Chlorella vulgaris* give it a privileged position in the literature on optical measurement and remote sensing (Witkowski et al., 1994; Baránková et al., 2020).

* Correspondence: pyildiz@sinop.edu.tr

As light traverses the water column and encounters an interface, it may be reflected, transmitted, scattered, or absorbed. In the interaction of light with suspended particles, photons can be partially absorbed by pigments (e.g., chlorophyll-a or carotenoids) or redirected by intracellular structures such as grana, thylakoids, and chloroplast membranes, thereby producing scattering (Kirk, 1983; Witkowski et al., 1994). Scattering efficiencies are related to the particle radius r by Mie theory, which is also known as the scattering function of the size parameter $x = 2\pi r/\lambda$ (r: particle radius, λ: wavelength), and the particle's refractive index. In practice, Mie scattering dominates according to particle sizes with size parameters of $0.1 \leq x \leq 50$, which corresponds to particle radii in the visible range of approximately 0.05–5 µm. Other scattering behaviors include Rayleigh scattering and geometrical optics scattering, and their limits are $x \leq 0.1$ and $x \geq 50$, respectively.

In recent decades, the remote sensing of inland waters has advanced considerably. Biooptical models originally designed for Case-1 oceans (optically simple open-ocean waters where variability is mainly driven by phytoplankton) fail to represent optically complex lakes where CDOM, suspended sediments, and phytoplankton collectively influence spectral reflectance (Giardino et al., 2014; Spyrakos et al., 2018). Numerous algorithms have since been proposed to estimate chlorophyll-a in optically complex inland waters from Earth observation data (Neil et al., 2019; Werther et al., 2025). Backscattering and absorption jointly explain over 90% of remote sensing reflectance variability, highlighting the need for in situ optical validation (Shi et al., 2014; Dörnhöfer et al., 2016). In spite of these advances, however, there is still a need for multiangle and hyperspectral in situ scattering observations in freshwaters for better modeling of absorption and scattering in optically diverse inland waters. To address the need for low-cost and robust field-deployable instruments for establishing dense in situ observation networks, a prototype goniometer with high spectral resolution was built and tested using *C. vulgaris*. In this study, we describe the instrument and the data processing algorithm and we present the results.

1.1. Background and research motivation

Experimental evidence consistently shows that scattering by algal cells is controlled by both their external morphology and internal structure. Early measurements (Table) highlighted the contribution of the cell wall to total scattering, while later work demonstrated that the internal structure plays a dominant role with scattering characteristics varying across the cell cycle (Quinby-Hunt et al. 1989; Witkowski et al., 1994; Baránková et al., 2020). Later studies extended this understanding by investigating angular dependencies. Laboratory measurements of

Table. Summary of the literature on scattering properties of particles and planktonic organisms.

Reference	Wavelengths (nm)	Angles	Organisms	Environment
Witkowski et al. (1994)	633	30°–120°	*Chlorella vulgaris*	Laboratory
Volten et al. (1998)	633	20°–160°	15 phytoplankton species, two silt types	Laboratory
Witkowski et al. (1998)	488, 514, 633	8°–155°	*Chlorella vulgaris*, *Chlorella kessleri*, *Chroococcus minor*	Laboratory
Vaillancourt et al. (2004)	440, 470, 510, 620	141°, 35°–144°	29 phytoplankton species + one heterotrophic bacterium	Laboratory
Chami et al. (2005)	443, 490, 555	0.6°–177.3°	Mineral particles, phytoplankton	In situ
O'Bree (2007)	633	5°–165°	Natural water samples (Gippsland Lakes, Great Barrier Reef)	Laboratory and in situ
Basedow et al. (2019)	443, 486, 551	141°	*Calanus finmarchicus* (zooplankton)	In situ and satellite
Baránková et al. (2020)	400–750	0° + integrating sphere	*Chlorella vulgaris* IPPAS-C1	Laboratory
Davies et al. (2021)	443, 488, 547, 670	0°–180°	Zooplankton (*Calanus* spp., krill), fish eggs, detritus	In situ and laboratory
Lomas et al. (2024)	375–730	104°, 130°, 141°, 151°	50+ phytoplankton strains (diatoms, dinoflagellates, cyanobacteria, etc.)	Laboratory
This study	423–728	0°–160°	*Chlorella vulgaris*	Laboratory

different phytoplankton species revealed strongly forward-direction phase functions and polarization maxima around 90°, confirming that both the scattering angle and the internal structure shape the observed patterns (Volten et al., 1998; Baránková et al., 2020). In contrast, backscattering efficiency was shown to depend on taxonomic composition and refractive index variability (Vaillancourt et al., 2004; O'Bree, 2007). These findings emphasize that the accuracy of scattering measurements depends on the geometry of the observation and the internal structural complexity of the particle.

Understanding the optic properties of microalgae is essential for accurately modeling the light distribution inside photobioreactors. These parameters determine how photons are redistributed within dense cultures and directly influence both photosynthetic efficiency and biomass productivity (Wheaton and Krishnamoorthy, 2012; Fuente et al., 2017). On the cellular scale, optical processes such as pigment absorption, refractive-index contrasts, and intracellular light redistribution shape the overall photic efficiency of microalgae (Lehmuskero et al., 2018). However, applications or devices capable of performing in situ measurements for spectral-angular behavior characterization of inland waters are needed. Such applications can be extended using the capabilities of instruments such as Sentinel-3 OLCI and PACE satellite sensors and unmanned aerial vehicles.

To address this gap, we developed a cost-effective in situ optical measurement system specifically designed for inland waters. The instrument measures detailed optical characterization across scattering angles of 0° to 160° and wavelengths of 423 to 728 nm, covering both visible and near-infrared regions. The system was first tested using monocultures of *C. vulgaris*, a well-studied model species for chlorophyll-a optical analysis. This system can provide high-resolution angular data aligned with the Sentinel-3 OLCI and NASA PACE spectral bands. Its use will support the establishment of a transferable framework for the ground truth and calibration of remote-sensing reflectance models and the characterization of optically diverse inland waters.

2. Materials and methods

A device was developed as a prototype of a relatively simple field-deployable sensor for the measurement of various constituents of inland waters. In the following subsections, the device set-up, the samples of *C. vulgaris* used to test the performance of the device, and the algorithms used in processing the raw data are described, respectively.

2.1. Set-up

We developed a spectral goniometer in house to measure transmittance/scattering at any angle with high spectral resolution. The set-up is shown in Figure 1. The system is installed in light-tight housing to block ambient light

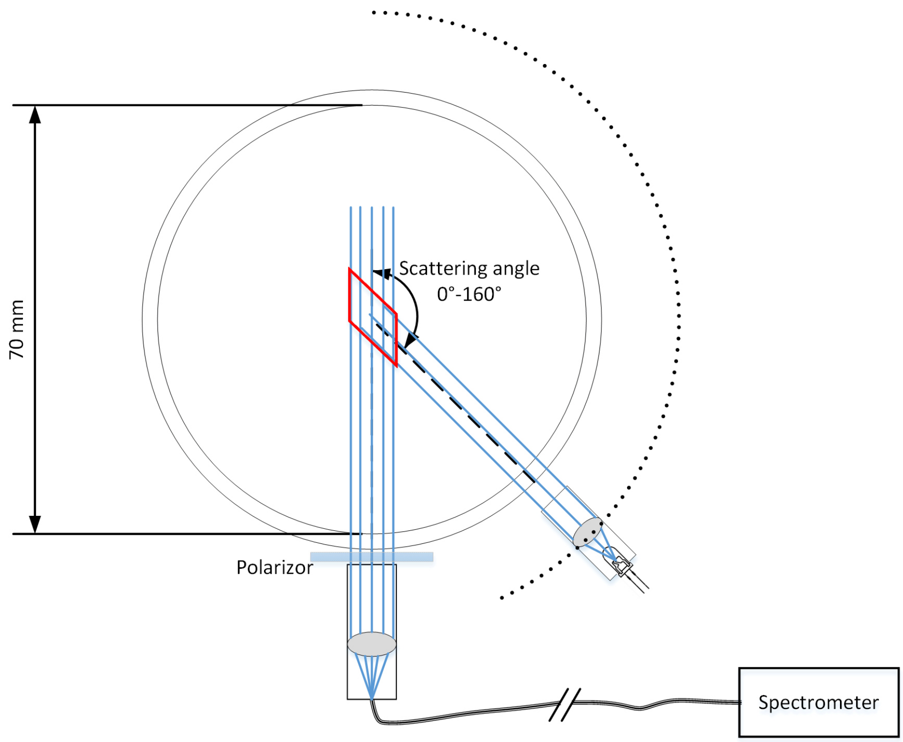

Figure 1. Schematic diagram of the spectral goniometer showing the illumination arm, sample chamber, and scattering geometry.

interference and ensure temperature stability. Spectral acquisition is performed using an ST-VIS-100 OEM spectrometer coupled via a QP400-2-VIS fiber-optic cable (Ocean Optics, Orlando, FL, USA) with core diameter of 400 μm and numerical aperture of 0.22. Light collection at the detector is achieved with an Ocean Optics 74-VIS collimating lens, while illumination is provided by a 12.7-mm EFL plano-convex lens (KPX513-C, Newport Corp., Irvine, CA, USA) coupled to a white LED light for a uniform visible spectrum. The spectrometer covers 350–810 nm with nominal spectral resolution of 6.3 nm and sampling interval of 0.3 nm; however, due to reduced signal-to-noise-ratios at both spectral ends, a usable range of 423–728 nm was selected for data processing.

The optical chamber, made of third-hydrolytic class soda-lime glass, has an inner diameter and path length of 71 mm, providing a balance between sufficient optical travel for clear water measurements and the avoidance of multiple scattering in dense samples. Both the LED current and the spectrometer exposure time are dynamically controlled to handle signal intensities within large dynamic ranges.

The basic design principle entails keeping the system simple and robust to allow dense monitoring networks in the future. The rotating light source can span an angle range of 0° to 160°. Although the servo can rotate in steps smaller than 1°, we use steps of 5° because, unlike typical Mie ripples observed with synthetic beads of a single size, the phase functions for real particles such as phytoplankton or silt with varying sizes, complex shapes, and nonuniform dielectric constants are relatively smooth and 5° sampling is better than the Nyquist rate. To avoid backlash, scans are always performed in the same rotational direction. A vertical or horizontal polarizing filter is optionally inserted in front of the collimator assuming the third and fourth parameters of the Stokes vector are zero (Li et al., 2020). For each measurement, a dark spectrum is recorded and subtracted automatically, and blank spectra (pure water) are obtained before each experimental series. Multiple repetitions are averaged to reduce noise and the entire process is fully automated through a custom controlled interface. The library of OceanDirect 3.1.0 (Ocean Optics, Orlando, FL, USA) is used for the automated acquisition of spectra from the spectrometer.

2.2. *Chlorella vulgaris* cultures

Chlorella vulgaris samples were obtained for this study from monoculture studies conducted in the Aquatic Research Laboratory of Hacettepe University's Faculty of Science, Department of Biology (Ankara, Türkiye). Cultures were grown in WC medium (Guillard and Lorenzen, 1972) at an initial cell density of 1295 cells mL^{-1} under cool-white LED illumination following a 12/12-h photoperiod. The temperature was maintained at 26 °C and cultures were continuously mixed by magnetic stirring in 250-mL Erlenmeyer flasks to ensure homogeneity and prevent cell sedimentation.

For morphological characterization and enumeration, fixed samples were sonicated for 3 min, followed by vortexing for another 3 min to ensure complete homogenization. The samples were then transferred to a Sedgewick–Rafter counting cell and allowed to settle for 10 min before imaging using a Leica 5000b microscope equipped with a C5 Flexacam (Leica Camera, Wetzlar, Germany). Due to inconsistencies in the automated cell-counting process, manual enumeration was performed using the multipoint tool in open-source ImageJ software. The total number of cells was counted from five randomly selected chambers (5 μL each) on the Sedgewick–Rafter slide. Based on microscopic measurements, the *C. vulgaris* cells exhibited nearly spherical shapes with diameters ranging between 4.0 and 8.75 μm (Figure 2). At 423 nm, the size parameter ranged from 29.7 to 65.0, whereas at 728 nm—the upper extreme of the measurement range—it ranged from 17.3 to 37.8. This means that scattering from the cell membrane was mostly within the Mie range, with the exception of large cells in shorter wavelengths slipping into the transition from Mie to geometric scattering. On the other hand, scattering from smaller structures inside the cell was well within the Mie range.

2.3. Data analysis

The data analysis workflow of this device is based on a physics-informed framework. The raw radiant flux measurements are corrected, normalized, and interpreted using radiative transfer principles and parametric scattering models such as the Henyey–Greenstein and Fournier–Forand models. This provides physical consistency with optical theory for all derived phase functions and polarization ratios.

For this reason, first, the raw radiant flux measurements are normalized because they are performed with different current levels and exposure durations. After subtracting dark spectra, blank spectra are used to calculate the correction coefficients for changes in light intensity and spectrum, and correction is applied. All measurements are then normalized to 1 ms assuming the linear response of the spectrometer.

Second, the phase function is estimated from the radiant flux measurements after subtraction of the dark spectra. In other words, it is necessary to solve for $\beta(\theta)$ in the following equation:

$$\Phi_e = \Phi_{e0} e^{-\mu z} \beta(\theta) = \Phi_{e0} e^{-\mu_a z} e^{-\mu_s z} \beta(\theta),$$

where Φ_{e0} is the incoming radiant flux, Φ_e is the radiant flux, μ_a is an absorption coefficient, μ_s is the scattering coefficient, $\mu = \mu_a + \mu_s$ is the attenuation coefficient, and z is the path length of the sample. Incoming radiant

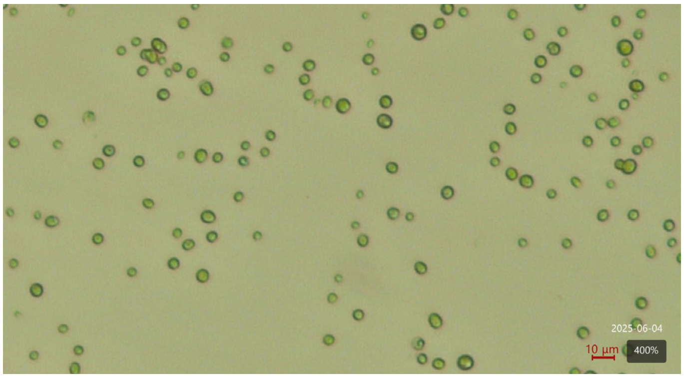

Figure 2. *Chlorella vulgaris* samples.

flux is estimated with blank water at a zero scattering angle. μ is solved at the same angle with the sample assuming a narrow reception angle so that only nonscattered light is measured at 0°. For other angles, $\beta(\theta)$ is solved after correcting for the volume of the parallelogram-shaped intersection shown in Figure 1 under the assumption that the average path length does not change with the angle.

Once the phase function is estimated at the relevant measurement angles, it is necessary to achieve a parametric fit to the phase function, or the volume scattering function (VSF), to interpolate between measurements and extrapolate toward 0° and 180°. The literature is rich in various parametric forms of such functions (Sharma, 2014). We tested the Henyey–Greenstein (Henyey and Greenstein, 1941) and double Henyey–Greenstein, Cornette–Shanks (Cornette and Shanks, 1992), Fournier–Forand (Fournier and Forand, 1994), and two-term Reynolds–McCormick (Harmel et al., 2021) functions. However, most of these functions performed poorly in representing the backscattering region. Therefore, a triple Henyey–Greenstein model was adopted, combining a double Henyey–Greenstein term with an additional Gaussian component to improve the fit for the backscattering lobe as follows:

$$\hat{\beta}(\theta) = A\left(f_1\, HG(\theta; g_1) + (1 - f_1)\, HG(\theta; g_2) + f_2\, G(\theta; \sigma^2)\right),$$

$$0 \le f_1 \le 1,\ 0 \le f_2,\ 0° \le \Theta \le 180°,$$

where

$$HG(\theta; g) = \frac{1 - g^2}{(1 + g^2 - 2g\cos(\theta))^{3/2}}$$

and

$$G(\theta; \sigma^2) = \frac{1}{\sqrt{2\pi\sigma^2}} e^{-\frac{(\theta - 180°)^2}{2\sigma^2}}.$$

In total, we have six parameters $(A, f_1, f_2, g_1, g_2,$ and $\sigma^2)$. It is possible to achieve a slightly better fit by increasing the number of parameters, but that may result in overfitting to unmodeled deviations.

For polarization, linear polarization is calculated as follows:

$$P_r = \frac{I_\perp - I_\parallel}{I_\perp + I_\parallel},$$

as suggested by Zubko and Chornaya (2019), where $I_\perp$ and $I_\parallel$ represent S-polarized and P-polarized measurements, respectively.

3. Results

To investigate the scattering geometry of *C. vulgaris* across different wavelengths and cell densities, a series of optical analyses were conducted. The measurements focused on quantifying angular and spectral variations that define the distribution and directionality of scattered light. Together, these analyses establish the foundation for interpreting the geometric and spectral characteristics of light scattering in *C. vulgaris* suspensions.

Angular linear polarization measurements at a wavelength of 450 nm were performed to determine the cell morphology of *C. vulgaris*. Linear polarization curves for different densities are shown in Figure 3. The polarization curves exhibited distinct angular dependence, with a maximum between 80° and 100° for all densities.

The logarithms of radiant flux measurements were obtained in three dimensions as a function of the wavelength and the scattering angle (Figure 4). The angular-spectral scattering surfaces of *C. vulgaris* revealed consistent forward-scattering dominance across all cell concentrations, characteristic of particles scattering within the Mie range. Scattering intensities peaked at small angles (0° to 30°, forward direction) and diminished with backward direction. As cell concentration increased from $D_{cv}/8$ to D_{cv}, the overall scattering magnitude rose and the angular pattern broadened. Spectrally, decreases in scattering were observed near the absorption bands of chlorophyll-a, around 440 nm and 670 nm, where pigment absorption was maximum, while intensities were elevated in the near infrared region where absorption was

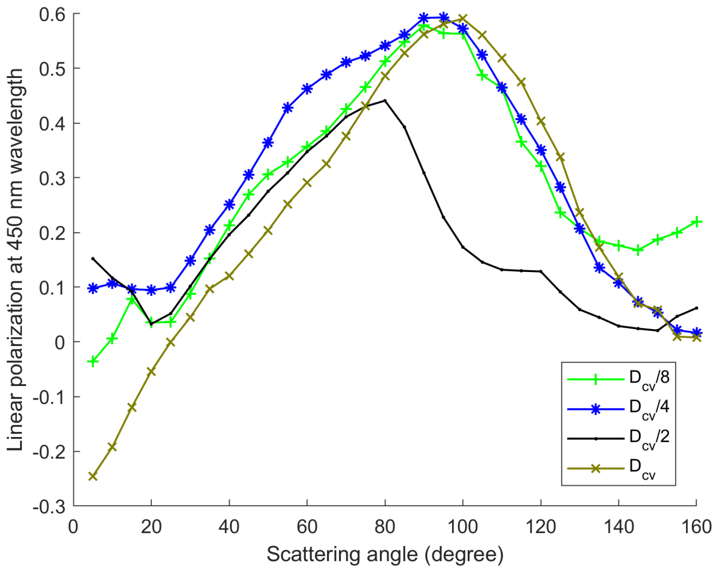

Figure 3. Linear polarization as a function of scattering angle at wavelength of 450 nm under increasing cell densities ($D_{cv}/8$ = 162 cells mL^{-1}, $D_{cv}/4$ = 324 cells mL^{-1}, $D_{cv}/2$ = 648 cells mL^{-1}, D_{cv} = 1295 cells mL^{-1}).

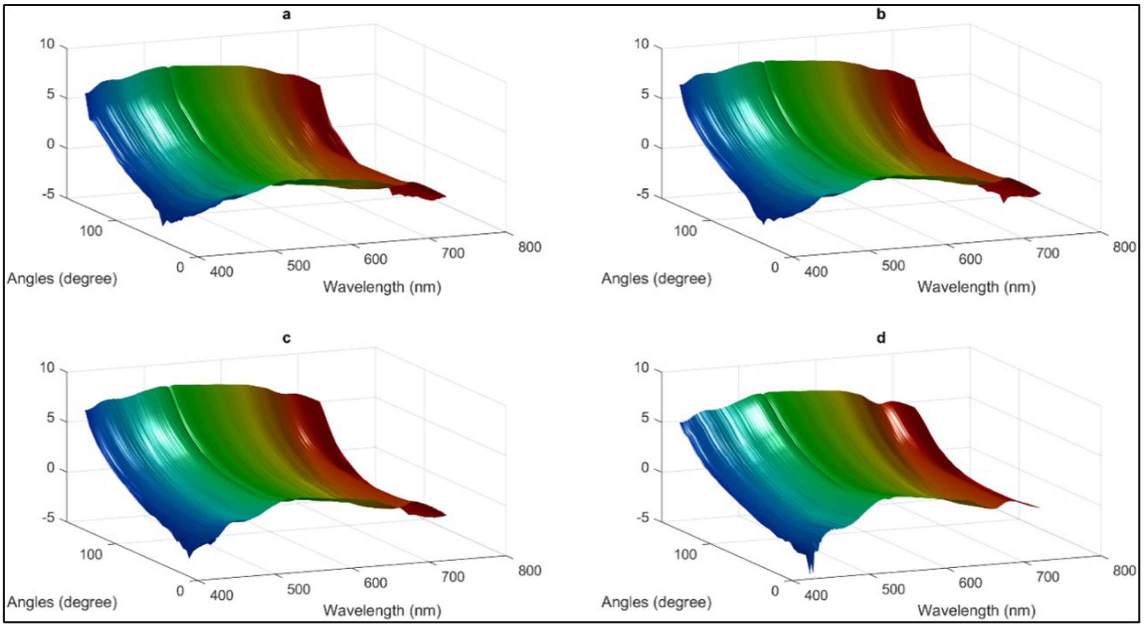

Figure 4. Three-dimensional views of angular-spectral measurements of *Chlorella vulgaris* cultures at four cell concentrations (a: $D_{cv}/8$, b: $D_{cv}/4$, c: $D_{cv}/2$, and d: D_{cv}). Z-axes illustrate the logarithm of the radiant flux.

minimum. This behavior shows that *C. vulgaris* exhibited wavelength-specific optical behavior characteristics of algal concentration and pigment absorption.

In the logarithmic polar plots of radiant flux in the wavelength band of 714–718 nm (Figure 5), the absorption of chlorophyll-a is seen to be negligible and the curve shape is similar to that of the corresponding phase function. The VSF curves of *C. vulgaris* showed a distinct forward-direction peak distribution characteristic of Mie scattering in algal cells. The scattering intensity increased monotonically with increasing cell density, while the angular pattern maintained its overall shape at all density levels.

The VSF angular profiles exhibited a clear forward-direction distribution for all wavelengths, with intensity and angular breadth increasing with *C. vulgaris* density.

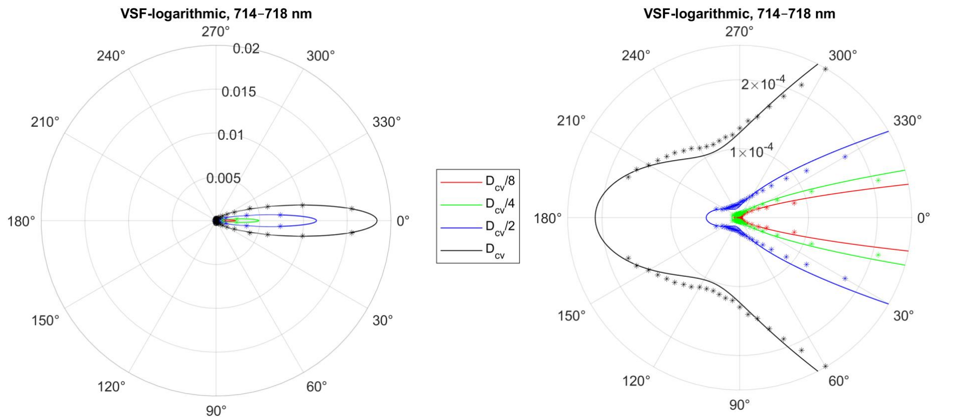

Figure 5. Volume scattering functions (VSFs) of *Chlorella vulgaris* measured in the 714–718 nm band for four cell densities of *Chlorella vulgaris* (D_{cv}: density of *C. vulgaris*). Left: Complete angular distribution from 0° to 160° on a logarithmic scale. Right: Close-up view of the backscattering region.

Spectrally, longer wavelengths (665–708 nm) showed wider scattering amplitudes, while shorter wavelengths (442–560 nm) maintained similar angular shapes but had lower overall magnitudes. At the lowest density (Figure 6a), the curves were narrowly confined near 0°, while with increased density (Figures 6b–6d) the magnitude and angular extent of the forward lobe expanded, particularly at longer wavelengths of ≥665 nm. At the highest density (Figure 6d), a distinct wavelength-dependent pattern emerged; 442 nm remained the most confined, whereas 708 nm formed the widest and most intense lobe.

Figure 7 illustrates how radiant flux changed with increasing *C. vulgaris* density. In low absorption bands such as those at 681 or 709 nm, the function was strictly monotonically increasing. Hence, estimating the density from the measurements was possible. At up to 324 cells mL^{-1}, they are almost linear. However, for high absorption bands such as 510–620 nm, the derivative becomes negative somewhere around 648 cells mL^{-1}.

4. Discussion

Optical methods that are used in the exploration of marine environments have also been employed for inland water ecosystems. However, it has become clear that, due to the different optical properties of marine and freshwater bodies, differentiated methods need to be used. Most estimations are performed using large databases thanks to the free and open data policy of the U.S. Geological Survey. Nevertheless, it has been noted that most prediction methods are statistical. Therefore, the accuracies are not yet at the desired level. Consequently, deriving IOPs from in situ measurements is considered a promising approach to address many of these issues, and recent efforts have increasingly focused on physics-informed techniques (Raissi et al., 2019; Topp et al., 2020). Considering all these factors together, especially in cases of remote sensing with large amounts of data, estimations might approach the accuracy rate of laboratory conditions with the use of physics-informed models. In this context, the present study has provided laboratory measurements of the optical properties of *C. vulgaris*. It was selected as a well-characterized, nearly spherical optical reference to validate the angular, spectral, and polarimetric responses of the proposed measurement system before applying the system to mixed and morphologically diverse particle assemblages.

The linear polarization curves peaked around a scattering angle of 90° (Figure 3). This plot is compatible with the spherical cell morphology of *C. vulgaris* with simulated and measured scattering (Quinby-Hunt et al., 1989) and that of other phytoplankton (Volten et al., 1998; Witkowski et al., 1998). For the least dense sample, we observed negative values at very small scattering angles. This may have been caused by unwanted reflections from the wall of the chamber, the magnitude of which could have been comparable to that of the actual signal.

Particle density and spectral absorption features significantly influence scattering behavior in *C. vulgaris* as shown in Figure 4. Across all four density levels, the scattering showed a clear angular trend; values were maximum at small scattering angles and decreased toward larger angles. As the density of *C. vulgaris* increased, the overall scattering level rose and the angular gradient became less steep. Thus, at high concentrations, the differences between the forward and larger angles decreased. These findings are consistent with those of previous studies that specifically focused on microalgal absorption and scattering behavior (Witkowski et al., 1994; Volten et al., 1998; Baránková et al., 2020), supporting the optical behavior observed across varying concentrations in the present study.

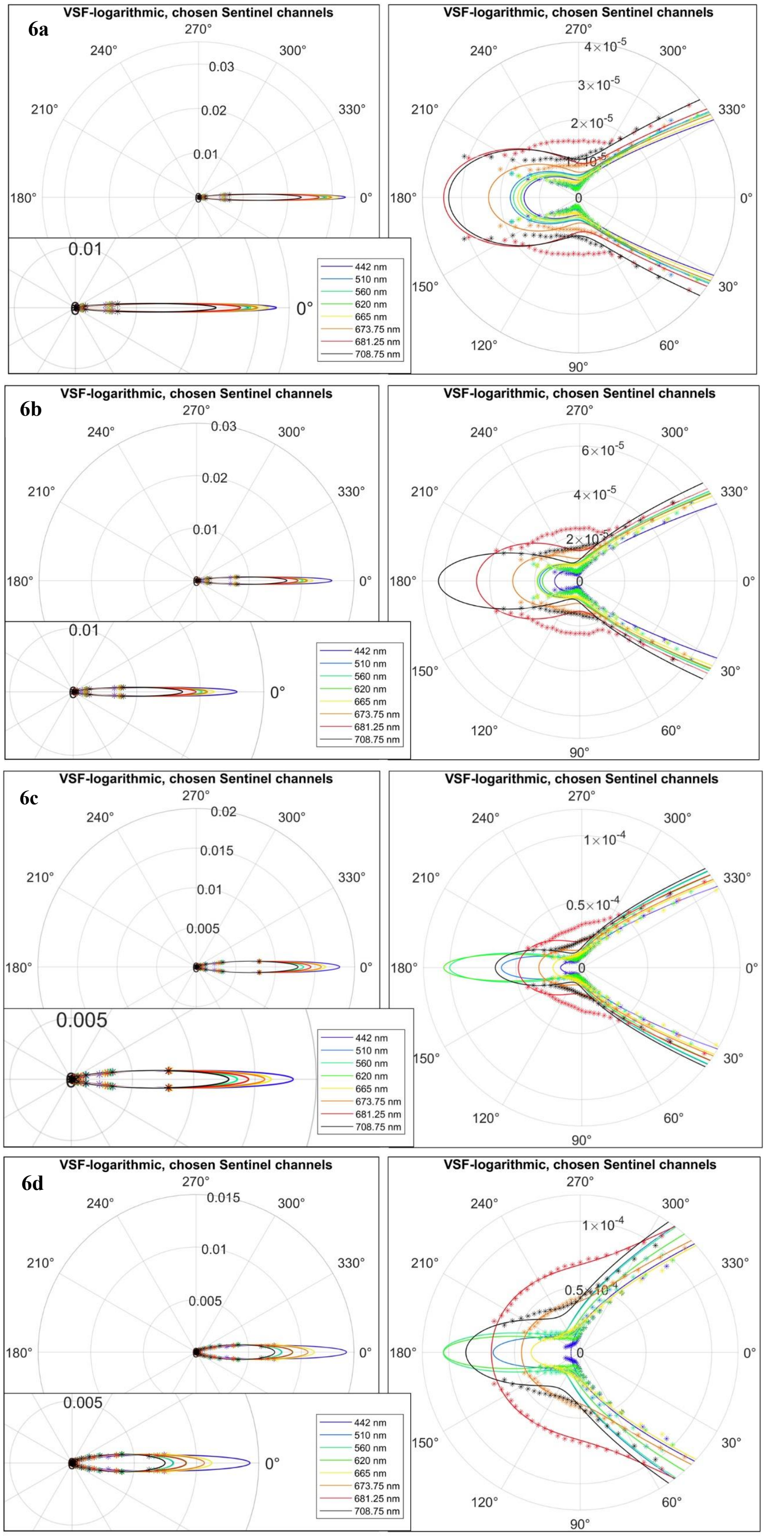

Figure 6. Volume scattering function (VSF) of *Chlorella vulgaris* at different cell densities from a) $D_{cv}/8$, b) $D_{cv}/4$, c) $D_{cv}/2$, and d) D_{cv} across the Sentinel-3 OLCI spectral band. Each polar plot shows the angular VSF (0° to 180°) on a logarithmic scale. The backscattering lobe becomes broader and more intense with increasing density while backscattering gradually rises, reflecting enhanced multiple scattering and increased optical density.

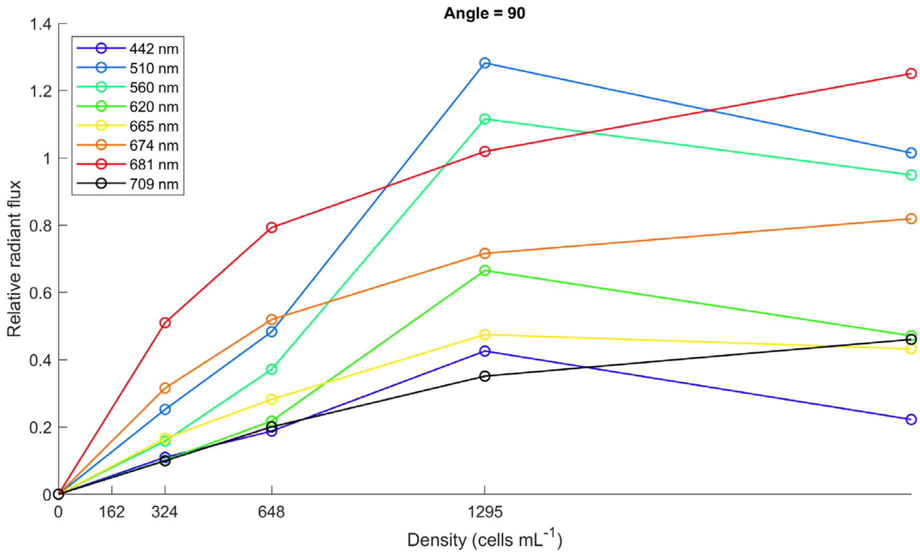

Figure 7. Radiant intensity at 90° scattering angle as a function of *Chlorella vulgaris* relative density at chosen Sentinel-3 band centers.

According to Mie theory, as particle size increases, the scattering intensity becomes increasingly concentrated in the forward direction. *C. vulgaris* typically exhibits cell diameters of 2–10 µm (4–8.75 µm in this study), and these dimensions place the cells within the Mie range for visible wavelength, where a forward scattering peak is expected (Figure 5). Our findings corroborate this behavior as the forward lobe became broader with increasing density, while the magnitude rose with the cell density. In the backscattering region, differences between densities became more pronounced, as shown in the right panel of Figure 5. While low-density samples exhibited weak and narrow lobes, high-density samples generated broader lobes with higher amplitudes, indicating a shift from single to multiple scattering conditions (Quinby-Hunt et al., 1989; Mobley, 1994). Complete VSF angular profiles across the near-infrared band primarily reflected scattering patterns rather than absorption, making them particularly suitable for inverse modeling based on Mie theory. Across all cell densities, the VSF profiles of *C. vulgaris* were strongly in the forward direction, consistent with Mie scattering behavior for particles whose radii of approximately 2–7 µm are comparable to visible wavelengths (Svensen et al., 2007; Gaigalas et al., 2009). At the lowest density (D_{cv}/8), scattering was narrowly confined to the range of 0° to 20°, indicating the dominance of single scattering by individual cells. Shorter wavelengths produced steeper angular decays, while longer wavelengths exhibited smoother transitions and higher relative magnitude. These findings indicate reduced pigment absorption and longer effective photon path lengths. The spectral asymmetry agrees with theoretical and empirical descriptions of phytoplankton optical behavior (Kirk, 1983; Baránková et al., 2020). At the highest density (D_{cv}), the 708-nm curve extends farthest outward, confirming that near-infrared scattering dominates where pigment absorption is minimal at high optical thickness (optical depth). Such sensitivity of angular scattering to both particle density and wavelength suggests that VSF-based inversion models or dynamic sensor systems could effectively distinguish optical regimes across inland waters with different trophic and turbidity conditions.

In Figure 7, 90° flux variations indicate that the scattered light first increases and then decreases as *C. vulgaris* density increases. At low densities, the scattered light increases linearly with the density. At higher densities, multiple scattering breaks the linear rule (Myers et al., 2013). At even higher densities, absorptions start to dominate and the derivative of the curve enters the negative zone. In Figure 7, we observe this phenomenon in high absorption bands. Since the dynamic range of optically complex inland waters (e.g., from eutrophic to ultraoligotrophic turbid waters with high organic content to very clear blue water) is typically very large (Spyrakos et al., 2018; Kerrisk et al., 2023), instruments with fixed path lengths may be insufficient. This highlights the need for adaptive sensor systems and algorithms capable of adjusting their dynamic ranges to effectively capture the variability in optically complex inland waters.

Given that the 718-nm VSF measurements were performed under conditions free of CDOM or other colored particulates, the resulting dataset provides a reference baseline for future spectral unmixing and optical modeling studies. Based on these data, future work will focus on particle-size estimation from scattering geometry, concentration measurements, and model validation using Mie-based inversion techniques.

Our experiments with *C. vulgaris* reveal some limitations of the current device prototype. The first limitation is due to fixed path lengths that cannot handle the large dynamic range of optical densities in inland waters. Second, the maximum scattering angle of 160° limits the accuracy of the fit to the backscattering lobe. Similarly, the smallest angle used for estimating the forward lobe could be even smaller with better collimation of the light source. However, the forward lobe fit is good and that may not be necessary.

Another point that should be considered in future work is the effect of the shape of scattering particles. The present study was intentionally limited to *C. vulgaris*, a nearly spherical species, whereas natural phytoplankton communities exhibit a wide range of nonspherical morphologies. Several studies have modeled phytoplankton using nonspherical shapes such as spheroids, cylinders, or concentric spheres, for which exact analytical solutions are available (Gibson et al. 2007; Nousiainen et al., 2012; Zhou et al., 2012). Approximate scattering solutions have also been developed for more complex and irregular particle shapes (Martin, 1993; Mishchenko, 2000; Nousiainen et al., 2012; Sánchez and Piera, 2016; Zhang et al., 2025). While studies are being conducted on realistic models of phytoplankton (Sun et al., 2024), it is expected that more accurate simulations will be possible in the near future as model development progresses. Previous studies suggest that particle shape has a limited influence on the spectral distribution of scattered light, whereas angular and polarimetric characteristics, particularly at larger scattering angles, are more sensitive to morphological differences (Zugger et al., 2008; Zhou et al., 2012). Considering the literature, it can be concluded that the developed device can be used for discriminating nonspherical particles, but a large number of experiments with various plankton species and nonorganic particles are necessary.

Calibration experiments using monodisperse microspheres, further design simplifications for field-robust operation, and trials with diverse particle types including phytoplankton, zooplankton, silt, and mixed suspensions are needed. Extending the angular range beyond 160° and improving the collimation and modeling of the intersection volume will further enhance retrieval accuracy. As a result of the laboratory measurements of *C. vulgaris* monocultures using the spectral goniometer, forward and backward scattering profiles were modeled. In particular, the polarization characteristics at 90°, three-dimensional patterns, VSFs, and radiant intensities at 90° across Sentinel-3 OLCI bands toward density changes were validated using physics-informed optical methods. The results confirmed Mie scattering dominance in line with the theoretical expectations. This modeling of the optical properties of *C. vulgaris* can be used for spectral unmixing studies and the optimization of sensors that use spectral-angular scattering profiles for in situ measurements. While the results of this study are promising, it is clear that other inland water components such as silt and detritus should also be modeled with cost-effective devices. With a broad range of scattering models, cost-effective devices with dynamic pathlengths can be used for the optic characterization of specific inland waters.

Acknowledgments
This study was supported by The Scientific and Technological Research Council of Türkiye (TÜBİTAK) with project number 123C130. The authors also thank Dr. Fatih Mangıt and Umut İplikci for providing the microalgal culture.

Author contributions
Pınar GÜRBÜZER: conceptualization, data curation, funding acquisition, investigation, methodology, writing – original draft, writing – review and editing.
Uğur Murat LELOĞLU: conceptualization, data curation, formal analysis, funding acquisition, methodology, software, validation, writing – original draft, writing – review and editing.

All authors have read and agreed to the published version of the manuscript.

References

Adjovu GE, Stephen, H, James, D, Ahmad S (2023). Overview of the application of remote sensing in effective monitoring of water quality parameters. Remote Sensing 15 (7): 1938. https://doi.org/10.3390/rs15071938

Bаránková B, Lazár D, Nauš J, Solovchenko A, Olga Gorelova O et al. (2020). Light absorption and scattering by high light-tolerant, fast-growing *Chlorella vulgaris* IPPAS-C1 cells. Algal Research 49: 101881. https://doi.org/10.1016/j.algal.2020.101881

Basedow SL, McKee D, Lefering I, Gislason A, Daase M E et al. (2019). Remote sensing of zooplankton swarms. Scientific Reports 9 (1): 686. https://doi.org/10.1038/s41598-018-37129-x

Brezonik, P, Menken KD, Bauer M (2005). Landsat-based remote sensing of lake water quality characteristics, including chlorophyll and colored dissolved organic matter (CDOM). Lake and Reservoir Management 21 (4): 373-382. https://doi.org/10.1080/07438140509354442

Chami M, Shybanov EB, Churilova TY, Khomenko GA, Lee MEG et al. (2005). Optical properties of the particles in the Crimea coastal waters (Black Sea). Journal of Geophysical Research: Oceans 110 (C11). https://doi.org/10.1029/2005JC003008

Cornette WM, Shanks JG (1992). Physically reasonable analytic expression for the single-scattering phase function. Applied optics 31 (16): 3152-3160. ttps://doi.org/10.1364/AO.31.003152

Davies EJ, Basedow SL, McKee D (2021). The hidden influence of large particles on ocean colour. Scientific Reports 11 (1): 3999. https://doi.org/10.1038/s41598-021-83610-5

Dörnhöfer K, Göritz A, Gege P, Pflug B, Oppelt N (2016). Water constituents and water depth retrieval from Sentinel-2A—a first evaluation in an oligotrophic lake. Remote Sensing 8 (11): 941. https://doi.org/10.3390/rs8110941

Fournier GR, Forand JL (1994). Analytic phase function for ocean water. Ocean Optics XII 2258: 194-201. https://doi.org/10.1117/12.190063

Fuente D, Keller J, Conejero JA, Rögner M, Rexroth S et al. (2017). Light distribution and spectral composition within cultures of microalgae: quantitative modelling of the light field in photobioreactors. Algal Research 23: 166-177. https://doi.org/10.1016/j.algal.2017.01.004

Gaigalas AK, He H-J, Wang L (2009). Measurement of absorption and scattering with an integrating sphere detector: application to microalgae. Journal of Research of the National Institute of Standards and Technology 114 (2): 69-81. https://doi.org/10.6028/jres.114.006

Giardino C, Bresciani M, Stroppiana D, Oggioni A, Morabito G (2014). Optical remote sensing of lakes: an overview on Lake Maggiore. Journal of Limnology 73 (S1): 201-214. https://doi.org/10.4081/jlimnol.2014.817

Gibson RN, Atkinson RJA, Gordon JDM (2007). Oceanography and Marine Biology: An Annual Review. Boca Raton, FL, USA: CRC Press. https://doi.org/10.1201/9781420050943

Guillard RRL, Lorenzen CJ (1972): Yellow-green algae with chlorophyllide c. Journal of Phycology 8: 10-14.

Harmel T, Agagliate J, Hieronymi M, Gernez P (2021). Two-term Reynolds–McCormick phase function parameterization better describes light scattering by microalgae and mineral hydrosols. Optics Letters 46 (8): 1860-1863. https://doi.org/10.1364/OL.420344

Henyey LG, Greenstein JL (1941). Diffuse radiation in the galaxy. Astrophysical Journal 93: 70-83.

Kerrisk G, Drayson N, Ford P, Botha H, Anstee J (2023). Performance assessment of serial dilutions for the determination of backscattering properties in highly turbid waters. Limnology and Oceanography: Methods 21 (5): 243-258. https://doi.org/10.1002/lom3.10542

Kirk JT (1983). Light and Photosynthesis in Aquatic Ecosystems. 1st ed. Cambridge, UK: Cambridge University Press.

Lehmuskero A, Chauton MS, Boström T (2018). Light and photosynthetic microalgae: a review of cellular- and molecular-scale optical processes. Progress in Oceanography 168: 43-56. https://doi.org/10.1016/j.pocean.2018.09.002

Li X, Luan X, Guo J (2020). Preliminary study on the polarization characteristics of volume scattering from planktonic algae. In: 24th National Laser Conference and Fifteenth National Conference on Laser Technology and Optoelectronics; Shanghai, China. pp. 898-903. https://doi.org/10.1117/12.2587666

Lomas MW, Neeley AR, Vandermeulen R, Mannino A, Thomas C et al. (2024). Phytoplankton optical fingerprint libraries for development of phytoplankton ocean color satellite products. Scientific Data 11 (1): 168. https://doi.org/10.1038/s41597-024-03001-z

Martin RJ (1993). Mie scattering formulae for non-spherical particles. Journal of Modern Optics 40 (12): 2467-2494. https://doi.org/10.1080/09500349314552471

Mishchenko MI (2000). Calculation of the amplitude matrix for a nonspherical particle in a fixed orientation. Applied Optics 39 (6): 1026-1031. https://doi.org/10.1364/AO.39.001026

Mobley CD (1994). Light and Water: Radiative Transfer in Natural Waters. San Diego, USA: Academic Press.

Myers JA, Curtis BS, Curtis WR (2013). Improving accuracy of cell and chromophore concentration measurements using optical density. BMC Biophysics 6 (1): 4. https://doi.org/10.1186/2046-1682-6-4

Neil C, Spyrakos E, Hunter PD, Tyler AN (2019). A global approach for chlorophyll-a retrieval across optically complex inland waters based on optical water types. Remote Sensing of Environment 229: 159-178. https://doi.org/10.1016/j.rse.2019.04.027

Nousiainen T, Zubko E, Lindqvist H, Kahnert M, Tyynelä J (2012). Comparison of scattering by different nonspherical, wavelength-scale particles. Journal of Quantitative Spectroscopy and Radiative Transfer 113 (18): 2391-2405. https://doi.org/10.1016/j.jqsrt.2012.03.032

O'Bree B (2007). Investigations of light scattering by Australian natural waters for remote sensing applications. PhD Thesis, Curtin University, Perth, Australia.

Quinby-Hunt MS, Hunt AJ, Lofftus K, Shapiro D (1989). Polarized-light scattering studies of marine Chlorella. Limnology and Oceanography 34 (8): 1587-1600. https://doi.org/10.4319/lo.1989.34.8.1587

Raissi M, Perdikaris P, Karniadakis GE (2019). Physics-informed neural networks: a deep learning framework for solving forward and inverse problems involving nonlinear partial differential equations. Journal of Computational Physics 378: 686-707. https://doi.org/10.1016/j.jcp.2018.10.045

Robinson C (2017). Phytoplankton biogeochemical cycles. In: Castellani C, Edwards M (editors). Marine Plankton: A Practical Guide to Ecology, Methodology and Taxonomy. Oxford, UK: Oxford University Press, pp. 249-257.

Safi C, Zebib B, Merah O, Pontalier P-Y, Vaca-Garcia C (2014). Morphology, composition, production, processing and applications of *Chlorella vulgaris*: a review. Renewable and Sustainable Energy Reviews 35: 265-278. https://doi.org/10.1016/j.rser.2014.04.007

Sánchez A-M, Piera J (2016). Methods to retrieve the complex refractive index of aquatic suspended particles: going beyond simple shapes. Biogeosciences 13 (14): 4081-4098. https://doi.org/10.5194/bg-13-4081-2016

Schiller H, Doerffer R (1999). Neural network for emulation of an inverse model operational derivation of Case II water properties from MERIS data. International Journal of Remote Sensing 20 (9): 1735-1746. https://doi.org/10.1080/014311699212443

Sharma SK (2014). A review of approximate analytic light-scattering phase functions. In: Kokhanovsky A (editor). Light Scattering Reviews 9: Light Scattering and Radiative Transfer. Berlin, Heidelberg, Germany: Springer Praxis Books, pp. 53-100. https://doi.org/10.1007/978-3-642-37985-7_2

Shi K, Li Y, Zhang Y, Li L, Lv H et al. (2014). Classification of inland waters based on bio-optical properties. IEEE Journal of Selected Topics in Applied Earth Observations and Remote Sensing 7 (2): 543-561. https://doi.org/10.1109/JSTARS.2013.2290744

Spyrakos E, O'donnell R, Hunter PD, Miller C, Scott M et al. (2018). Optical types of inland and coastal waters. Limnology and Oceanography 63 (2): 846-870. https://doi.org/10.1002/lno.10674

Sun X, Brewin RJW, Hacker C, Viljoen JJ, Li M (2024). Generating open-source 3D phytoplankton models by integrating photogrammetry with scanning electron microscopy. Frontiers in Microbiology 15: 1429179. https://doi.org/10.3389/fmicb.2024.1429179

Svensen Ø, Frette Ø, Erga SR (2007). Scattering properties of microalgae: the effect of cell size and cell wall. Applied Optics 46 (23): 5762-5769. https://doi.org/10.1364/AO.46.005762

Topp SN, Pavelsky TM, Jensen D, Simard M, Ross MRV (2020). Research trends in the use of remote sensing for inland water quality science: moving towards multidisciplinary applications. Water 12 (1): 169. https://doi.org/10.3390/w12010169

Vaillancourt RD, Brown CW, Guillard RRL, Balch WM (2004). Light backscattering properties of marine phytoplankton: relationships to cell size, chemical composition, and taxonomy. Journal of Plankton Research 26 (2): 191-212. https://doi.org/10.1093/plankt/fbh012

Wei Z, Yu Y, Yi Y (2025). Prediction of future chlorophyll-a concentrations in large eutrophic shallow lakes under multiple stressors. Earth's Future 13 (5): e2024EF005293. https://doi.org/10.1029/2024EF005293

Werther M, Burggraaff O, Gurlin D, Saranathan AM, Balasubramanian SV et al. (2025). On the generalization ability of probabilistic neural networks for hyperspectral remote sensing of absorption properties across optically complex waters. Remote Sensing of Environment 328: 114820. https://doi.org/10.1016/j.rse.2025.114820

Wheaton ZC, Krishnamoorthy G (2012). Modeling radiative transfer in photobioreactors for algal growth. Computers and Electronics in Agriculture 87: 64-73. https://doi.org/10.1016/j.compag.2012.05.002

Witkowski K, Król T, Lotocka M (1994). Light scattering matrix of Chlorella vulgaris cells and its variability due to cell modification. Oceanologia 36 (1): 19-31.

Witkowski K, Król T, Zieliriński A, Kuteń E (1998). A light-scattering matrix for unicellular marine phytoplankton. Limnology and Oceanography 43 (5): 859-869. https://doi.org/10.4319/lo.1998.43.5.0859

Volten H, De Haan JF, Hovenier JW, Schreurs R, Vassen W et al. (1998). Laboratory measurements of angular distributions of light scattered by phytoplankton and silt. Limnology and Oceanography 43 (6): 1180-1197. https://doi.org/10.4319/lo.1998.43.6.1180

Woolway RI, Zhang Y, Jennings E, Zohary T, Jane SF et al. (2025). Extreme and compound events in lakes. Nature Reviews Earth and Environment 6: 593-611. https://doi.org/10.1038/s43017-025-00710-w

Zhang Y, Yang P, Gao M, Zhang X (2025). Optical properties simulated for oceanic particles with nonspherical core-shell morphologies. Journal of Quantitative Spectroscopy and Radiative Transfer 338: 109400. https://doi.org/10.1016/j.jqsrt.2025.109400

Zhou W, Wang G, Sun Z, Cao W, Xu Z et al. (2012). Variations in the optical scattering properties of phytoplankton cultures. Optics Express 20 (10): 11189-11206. https://doi.org/10.1364/OE.20.011189

Zubko E, Chornaya E (2019). On the ambiguous definition of the degree of linear polarization. Research Notes of the AAS 3 (3): 45. https://doi.org/10.3847/2515-5172/ab0c11

Zugger ME, Messmer A, Kane TJ, Prentice J, Concannon B et al. (2008). Optical scattering properties of phytoplankton: measurements and comparison of various species at scattering angles between 1° and 170°. Limnology and Oceanography 53 (1): 381-386. https://doi.org/10.4319/lo.2008.53.1.0381